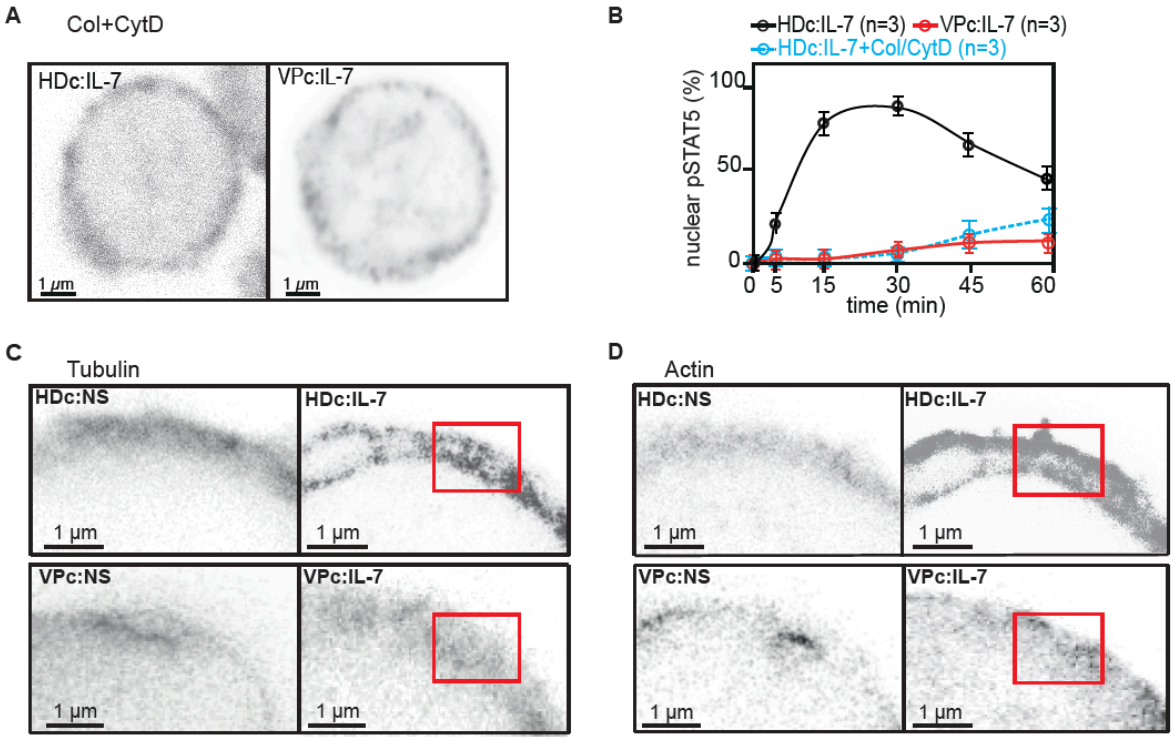

Supplemental Figure 1. Impaired cytoskeletal reorganization in CD4 T cells from HIV-infected patients.

(**A**) Effects of the colchicine plus cytochalasin D (Col+CytD) on the phosphorylation and STAT5 NT induced by IL-7 in HD CD4 T cells (HDc) compared to that induced by IL-7 in VP CD4 T cells (VPc). Representative cells among 50 cells per donor for HD (3 donors) and 15 to 50 cells for VP CD4 T cells (3 donors) are shown. (**B**) After IL-7 stimulation, the kinetics of pSTAT5 accumulation in the nucleus were measured in HD CD4 T cells (black line) and HD CD4 T cells treated with colchicine plus cytochalasin D (Col/CytD, blue line) and compared to those of IL-7-stimulated CD4 T cells from VPs (red line). pSTAT5 was quantified using ImageJ and the results are shown as the mean ± SD for three donors. (**C**, **D**) IL-7-induced reorganization of microfilaments and microtubules was followed by pulsed-STED microscopy. (**C**) Pattern obtained after anti-tubulin labelling. (**D**) Pattern obtained after anti-actin labelling. Representative images from the analysis of cells from three donors.

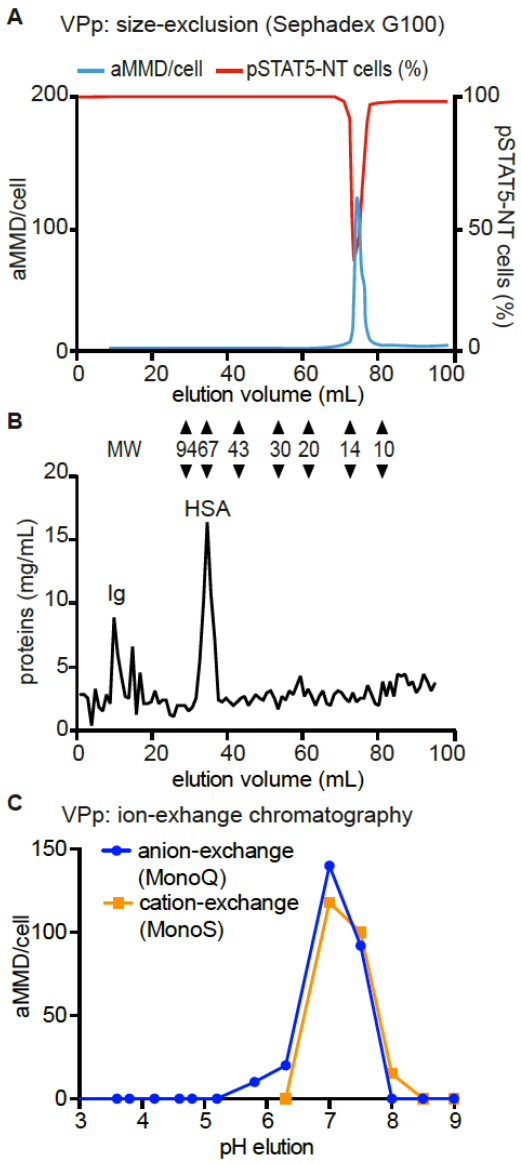

D Mass spectrometry results

	Mnemonic	ID	PI	MW	103-Unique	nXP-Unique	Score
1	PA21B_HUMAN	P04054	7.95	14138.99	31	7	0.640
2	TMEM9_HUMAN	Q9P0T7	6.23	18568.37	39	2	0.290
3	ESM1_HUMAN	Q9NQ30	6.83	18122.42	43	2	0.100
4	SSRB_HUMAN	P43308	7.03	18273.74	35	5	0.100
5	CYTD_HUMAN	P28325	6.76	13858.6	30	3	0.085
6	GPIX_HUMAN	P14770	6.14	17316.06	19	5	0.042
7	B2MG_HUMAN	P61769	6.07	11618.01	30	2	0.027
8	EPGN_HUMAN	Q6UW09	7.72	14724.99	38	1	0.025
9	IL19_HUMAN	Q9UHD0	7.8	17812.56	39	4	0.023
10	EREG_HUMAN	O14944	6.32	15099.25	33	5	0.020
11	GML_HUMAN	Q99445	6.67	15918.41	28	7	0.020
12	IL3_HUMAN	P08700	7.05	15091.38	28	3	0.020
13	VPREB_HUMAN	P12018	6.35	14534.23	32	3	0.020
14	PA2GX_HUMAN	O15496	6.48	18153.1992	33	5	0.020
15	CYTM_HUMAN	Q15828	7	13591.5	27	2	0.017
16	LV001_HUMAN	P04211	6.75	10239.39	9	0	0.010
17	NPC2_HUMAN	P61916	6.95	14578.79	27	2	0.007
18	IL2_HUMAN	P60568	7.05	15418.01	30	1	0.006
19	HV208_HUMAN	P04438	7.97	14365.35	28	1	0.005
20	IL22_HUMAN	Q9GZX6	7.1	16749.33	39	2	0.005

Supplemental Figure 2. Molecular characterization and identification of PLA2G1B in VP plasma.

(**A**) VP plasma was fractionated by gel filtration on a Sephadex G100 column. All fractions eluted from the column were tested for their ability to induce aMMDs (blue curve) and inhibit IL-7-induced pSTAT5 NT in HD CD4 T cells (red curve). (**B**) The level of total proteins in each fraction is represented in black. The line represents the mean values. Measurements were repeated with plasma from three VPs and three HDs. The signals obtained with HD plasma were subtracted for each experiment. (**C**) Active, 10 to 15 kDa, enriched fractions from Sephadex G100 columns were then used to frame the isoelectric point by retention on anion (MonoQ) or cation (MonoS) exchange columns followed by pH elution. The MMD-inducing activity of the various pH fractions was measured after adjusting their pH to 7.4. (**D**) The protein content of the gel filtration eluates (10-15 kDa) from HIV-infected patient plasma (3 donors) was analyzed by mass spectrometry and compared to the protein content of plasma from healthy donors (3 donors). Proteins were identified using the Mascot program (Matrix Science) against human proteins in the SwissProt database (Universal Protein Resource). Only the peptides providing the 20 most intense m/z peaks were automatically selected, fragmented, and sequenced (MS/MS). We thus calculated the excepted values for the 103 selected proteins to obtain the statistical weight of protein identification from the MS spectra series only, as described in the Supplemental material. The MS data were generated in triplicate from plasma samples of six blood donors: three HDs and three HIV-infected patients.

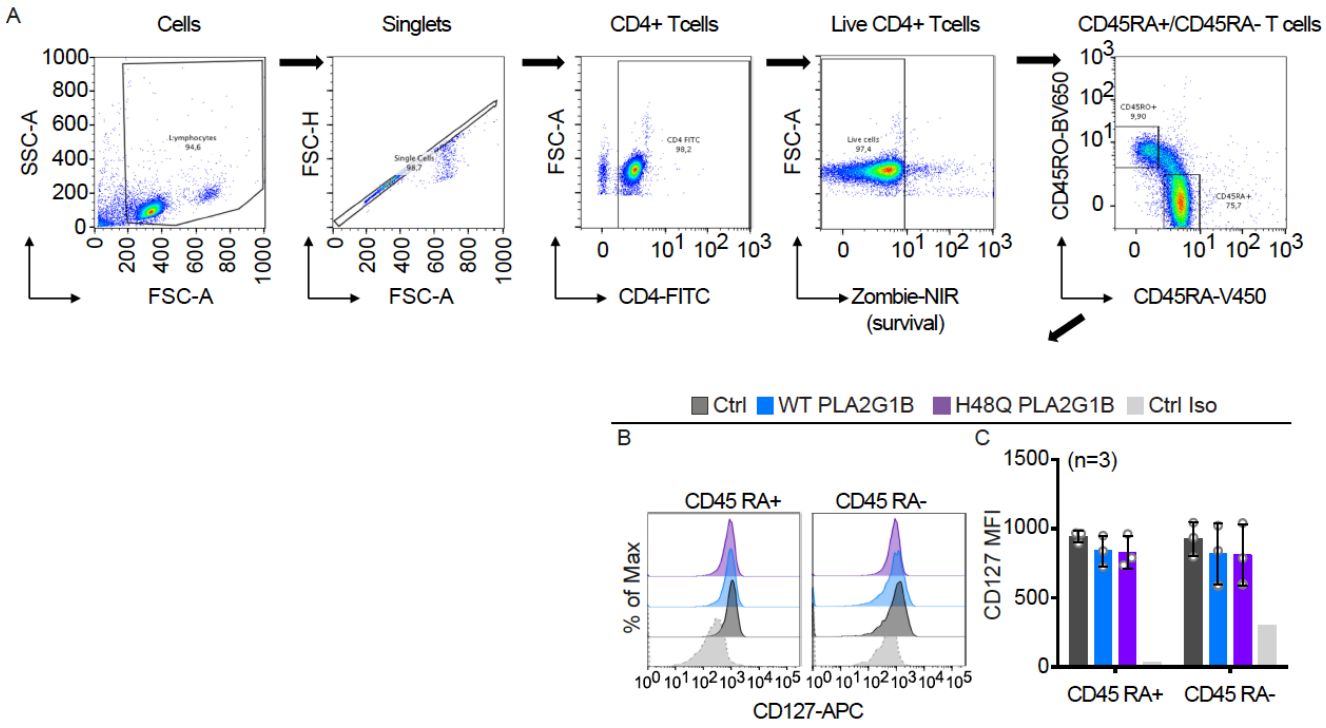

Supplemental Figure 3. The enzymatic activity of PLA2G1B does not change CD127 expression at the surface of CD45RA+ and CDR45RA- CD4+ T cells.

(**A**) Gating strategy used for FACS analysis of the effect of PLA2G1B on CD127 expression on CD45RA+ and CD45RA- CD4 T cells. (**B**) CD127 expression and (**C**) CD127 MFI on CD45RA+ and CD45RA- CD4 T cells after treatment with 1µM WT or H48Q PLA2G1B (n=3 donors).

Supplemental Figure 4. PLA2G1B induces the Bumpy phenotype on CD4 T cells but not CD8 T cells.

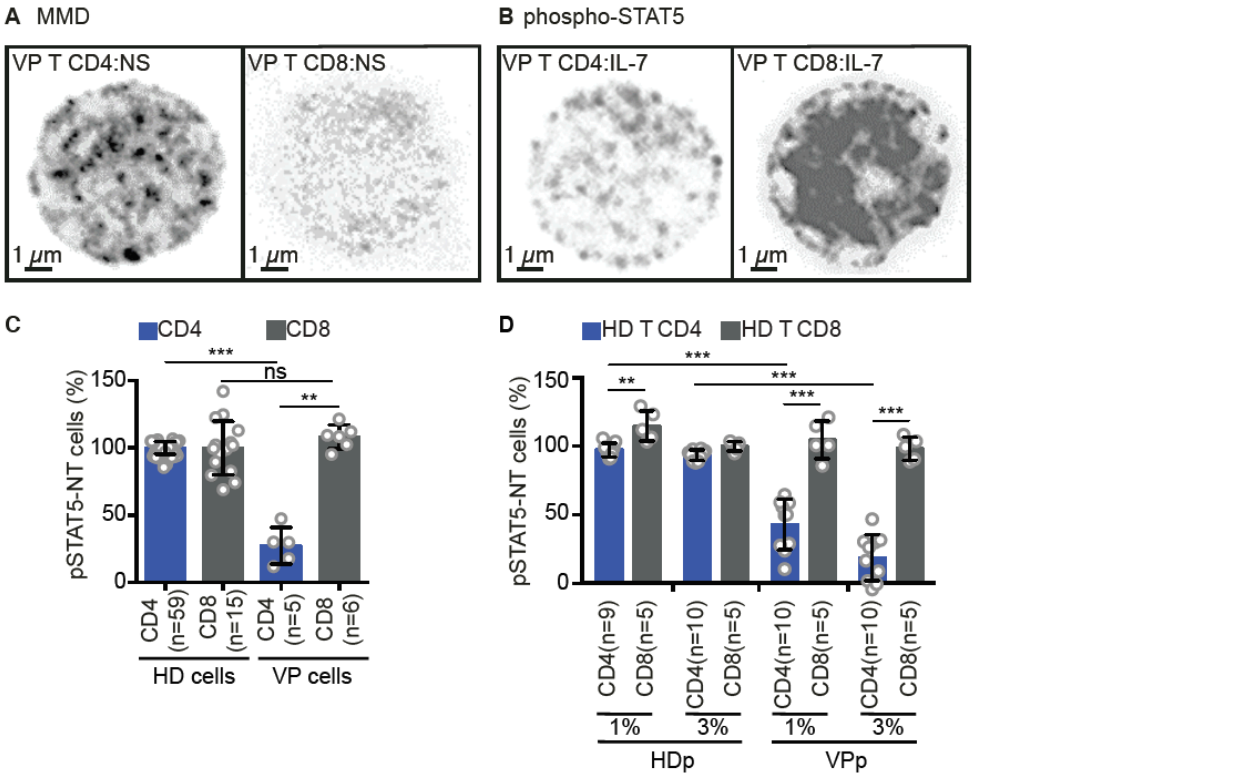

E Lipidomics analysis of HD CD4 and CD8 T cells

Lipid Name	CD4(n=3) (%)	CD8 (n=3) (%)	Fold CD4/CD8	p-value CD4 vs CD8
GM3 (d18:1/16:0)_C57H104N2O21	0,012	0,022	0,57	0,0278
GM3 (d18:1/24:1)_C65H118N2O21	0,011	0,021	0,53	0,0318
GM3(d18:1/24:0)_C65H120N2O21	0,005	0,012	0,42	0,0114
PC 36a:1_C44H86NO8P	1,627	1,879	0,87	0,0462
PC 36a:3_C44H82NO8P	2,793	2,327	1,20	0,0266
PC 37a:5_C45H80NO8P	0,057	0,069	0,83	0,0327
PC 38a:3_C46H86NO8P	0,669	0,590	1,13	0,0097
PC 38a:5_C46H82NO8P	2,286	2,168	1,05	0,0038
PE 38a:5_C43H76NO8P	0,805	0,892	0,90	0,0431
PE 42a:6_C47H82NO8P	0,005	0,008	0,61	0,0039
PI 36a:4_C45H79O13P	0,132	0,150	0,88	0,0400
PI 38a:5_C47H81O13P	0,277	0,305	0,91	0,0350
PI 40a:4_C49H87O13P	0,077	0,060	1,29	0,0431
PS 28a:2_C34H62NO10P	0,020	0,014	1,37	0,0178
PS 38a:1_C44H84NO10P	0,041	0,073	0,56	0,0379
PS 38a:5_C44H76NO10P	0,017	0,021	0,82	0,0238
PS 38a:6_C44H74NO10P	0,041	0,046	0,89	0,0078
PS 40a:1_C46H88NO10P	0,011	0,026	0,40	0,0140
PS 40a:7_C46H76NO10P	0,053	0,069	0,77	0,0131
SM (d18:1/C17:0)_C40H81N2O6P	0,054	0,048	1,13	0,0156
TG 53:1_C56H106O6	0,014	0,008	1,67	0,0064

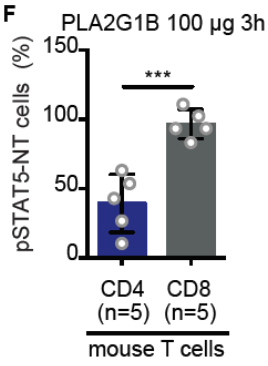

Supplemental Figure 4. PLA2G1B induces the Bumpy phenotype on CD4 T cells but not CD8 T cells.

(**A**) aMMDs on the surface of VP CD4 (n = 4) or CD8 (n = 4) T cells were labelled with cholera toxin and (**B**) pSTAT5 NT of IL-7-stimulated VP CD4 (n = 5) and CD8 (n = 6) T cells (2 nM, 15 min) from VPs was followed and analyzed by confocal microscopy. (**C**) IL-7-induced pSTAT5 NT was analyzed in CD4 and CD8 T cells from HDs (CD4 : n = 59, CD8: n = 15) and VPs (CD4: n = 5, CD8: n = 6). Results are shown as the pSTAT5-NT cells percentage normalized to the mean of the pSTAT5-NT response in CD4 T cells and CD8 T cells from HD, respectively. (**D**) IL-7-induced pSTAT5 NT was analyzed by confocal microscopy in HD CD4 (n = 9-10) and CD8 (n = 5) T cells after incubation with HDp or VPp (1 % and 3 %, 30 min). (**E**) Mass spectrometry analysis of the relative lipid content of HD CD4 and CD8 T cells (n = 3). Data are presented as the lipid species that are significantly and differentially present in CD8 T cells relative to CD4 T cells by a two tailed paired *t*-test among a total of 330 detected lipid species. (**F**) Effect of injecting 100 µg PLA2G1B for 3 h in C57BL/6 mice (5 mice from 1 experiment). The effect on CD8 T cells was compared to the effect on IL-7 CD4 T-cell response described in Figure 7K. The effects of PLA2G1B injections were evaluated by analyzing the ex vivo response (IL-7, 2 nM, 15 min, 37°C) of CD4 or CD8 T cells isolated from spleen (CD8 and pSTAT5 labelling analyzed by confocal microscopy). (**A**-**D** and **F**) Preparations were analyzed by confocal microscopy. An average of 200 cells were examined for each condition. Bar graphs show the mean ± SD. (**C**, **D** and **F**) Kruskal-Wallis test p-value was p=0.0003 in **C** and p<0.0001 in **D**; $^{**}p$<0.01 and $^{***}p$<0.001 by Mann-Whitney adjusted for multiple comparisons with p-value significant if p<0.0125 in **C** and p<0.00625 in **D**; $^{**}p < 0.01$ by unpaired *t*-test in **F.**

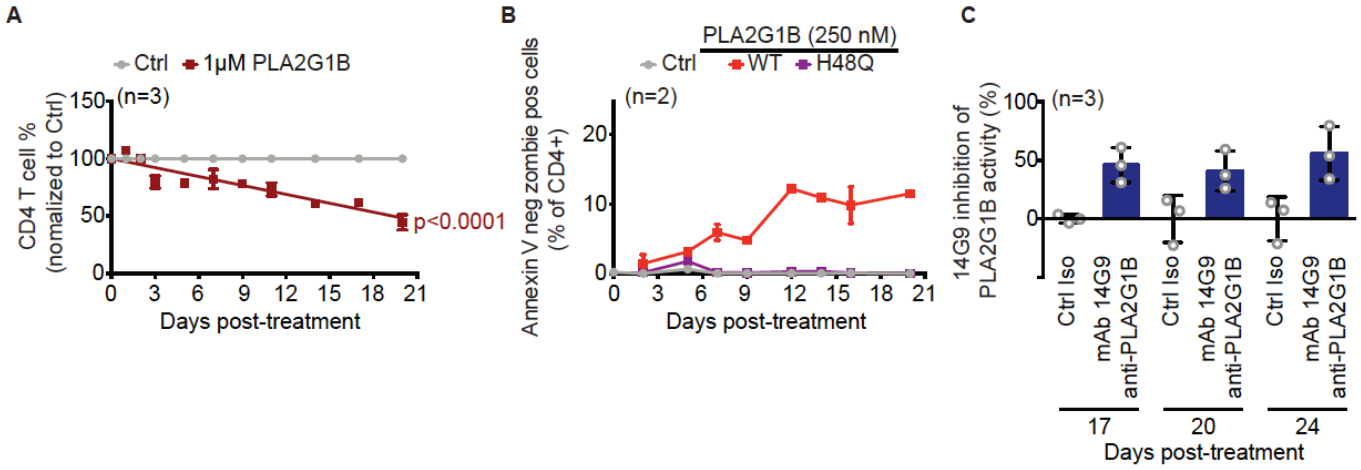

Supplemental Figure 5. The enzymatic activity of PLA2G1B is required to the induce Annexin V-negative Zombie-positive phenotype and cell death.

(**A**) PLA2G1B reduces the survival of human CD4 T cells. Cells were treated with PBS (Ctrl) or 1 µM of PLA2G1B (n = 3 donors). Results are shown as the mean ± SD of the percentage of CD4 T-cell counts normalized to the number of Ctrl cells at each time point. The lines show the linear regression and the p-value indicates the significance of difference with control. (**B**) The enzymatic activity of PLA2G1B is required to induce Annexin V-negative Zombie-positive CD4 T cells. FACS analysis of CD4 T cells for Annexin V-APC and Live/Dead Marker (Zombie-Violet) after treatment with PBS (Ctrl) or 250 nM of WT or H48Q PLA2G1B. Results are shown as the mean ± SD of the percentage of Annexin V-negative Zombie-positive CD4 T cells (n = 2 donors). (**C**) Anti-PLA2G1B mAb 14G9 decreases PLA2G1B-induced cell death of CD4 T cells. CD4 T cells were treated with PBS (Ctrl) or 250 nM of WT PLA2G1B with Control Isotype (0.67 µM) or anti-PLA2G1B mAb 14G9 (0.67 µM). The percentage of CD4 T-cell counts normalized to the number of Ctrl cells at each time point in presence of the control isotype (Ctrl Iso) or the 14G9 was measured for CD4 T cells from three donors. Results are shown as the mean ± SD of the percentage of inhibition of the effect of PLA2G1B on CD4 T-cell counts by the 14G9 relative to that by control isotype at days 17, 20, and 24 post-treatment.

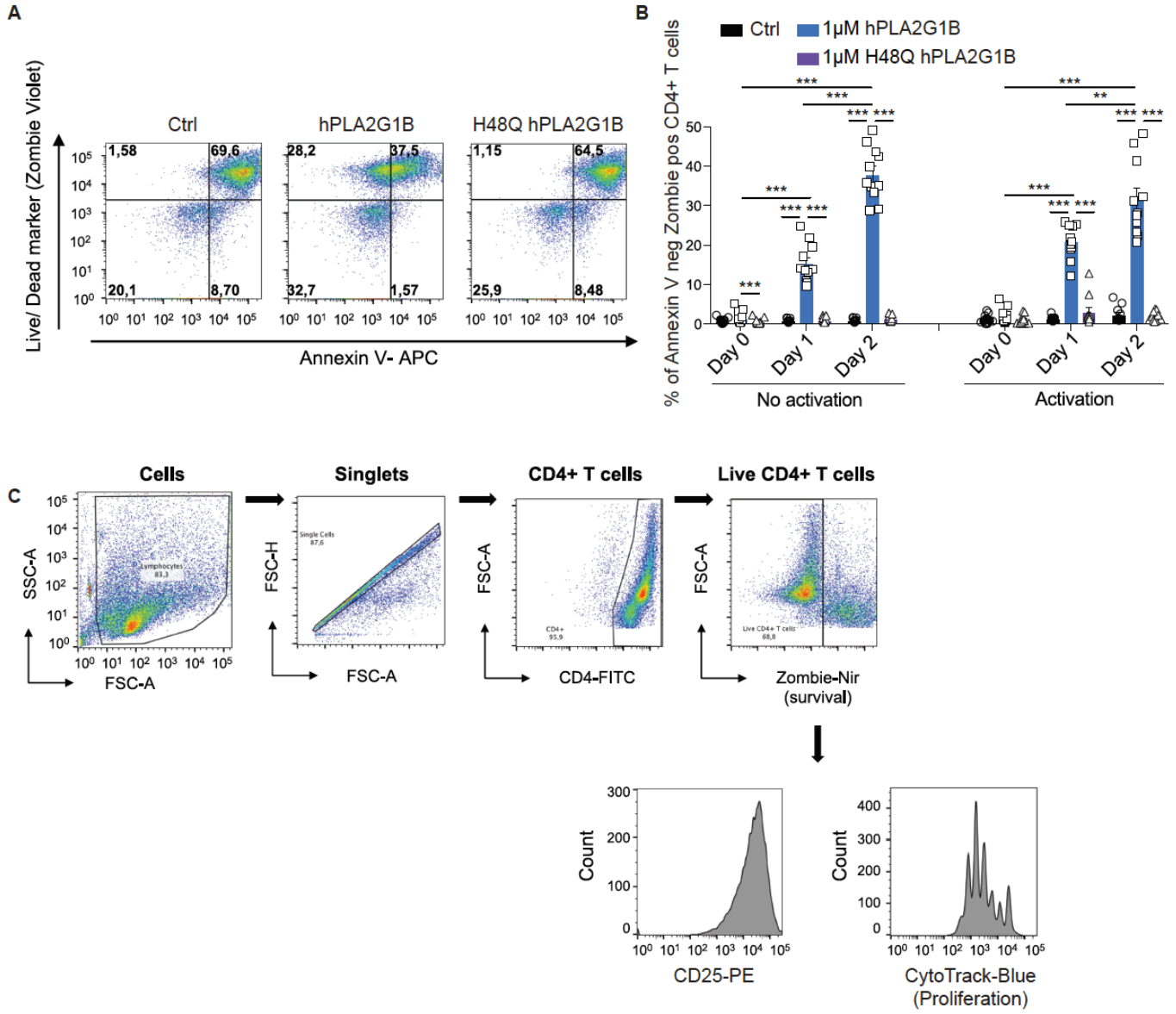

Supplemental Figure 6. PLA2G1B removes phosphatidylserine from the surface of dying mouse CD4 T cells.

(**A**, **B**) FACS analysis of mouse CD4 T cells for Annexin V-APC and Live/Dead Marker (Zombie-Violet) after treatment with 1 µM hPLA2G1B or H48Q. (**A**) Dot plots of activated murine CD4 T cells after 48 h of treatment with hPLA2G1B or H48Q. (**B**) Percentage of Annexin V-negative Zombie-positive CD4 T cells after activation and treatment with hPLA2G1B or H48Q (11 mice, n = 3 experiments). Kruskal-Wallis test $p<0.0001$, followed by Mann-Whitney test for multiple comparisons with adjusted p-value significant when $p<0.00278$: $^{**}p<0.00278$ and $^{***}p<0.001$. (**C**) Gating strategy used for FACS analysis of the effect of hPLA2G1B on mouse CD4 T cells after anti-CD3/CD28 and IL-2 stimulation (5 days) on CD25 expression and mCD4 T-cell survival and proliferation shown in Figure 7A-G.

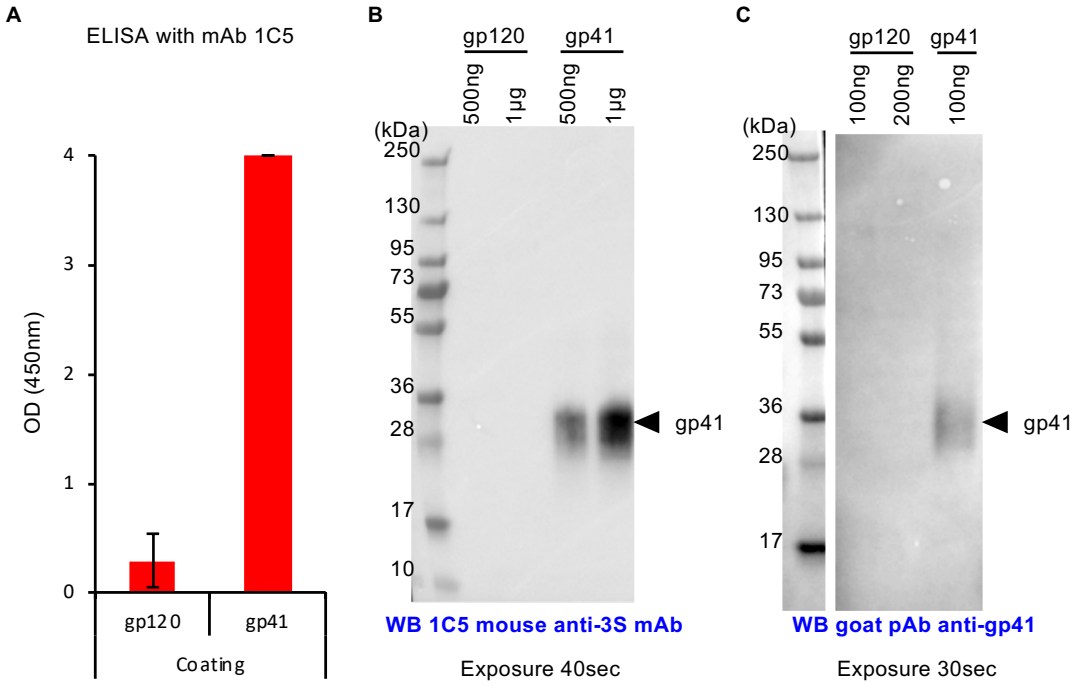

Supplemental Figure 7. Specificity of anti-3S 1C5 mAb and of anti-gp41 pAb.
(**A, B**) The anti-3S gp41 mAb 1C5 binds to gp41 but not gp120. (**A**) ELISA: the wells of microtiter plates were coated overnight with 10 µg of gp41 or gp120 recombinant proteins and binding of 1C5 (1 µg/well) to the proteins revealed with goat anti-mouse IgG-HRP. Results are shown as the mean ± SD of triplicates. (**B**) Immunoblot with the 1C5 mAb: 500 ng or 1 µg of gp120 or gp41 recombinant proteins was separated on 4%–20% Tris-Bis SDS-PAGE under reducing conditions and transferred to PVDF membranes. Antibody binding was tested at 1 µg/ml for 1C5. Antibody binding was revealed with goat anti-mouse IgG-HRP (1:10,000). (**C**) The goat anti-gp41 pAb binds to gp41 but not gp120. Immunoblot with anti-gp41 pAb: 100 and 200 ng gp120 or gp41 recombinant proteins was separated and transferred to PVDF membranes as above. Binding of anti-gp41 pAb (5 µg/ml) was revealed using donkey anti-goat IgG-HRP (1:10,000).

Supplemental Figure 8. Origin of PLA2G1B – Low expression levels in immune cells.

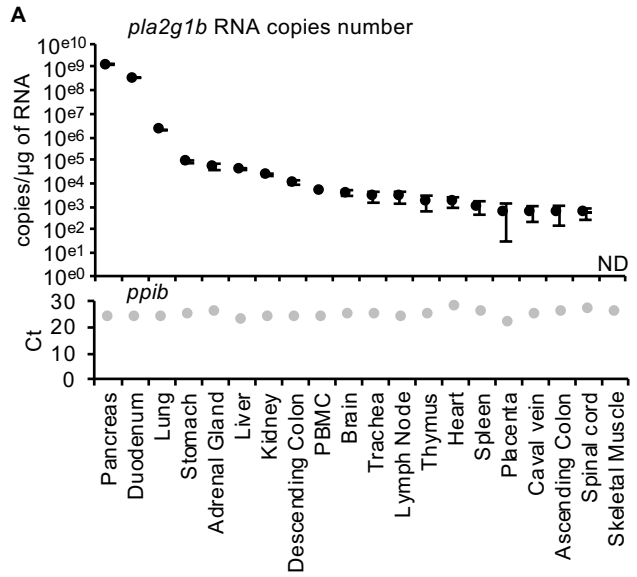

C

	Tissue type	
Adrenal	Fallopian tube	Skin
Bone Marrow	Heart. Ventricule. left	Rectum
Blood	Ileum	Spinal cord
Breast	Jejunum	spleen
Brain. Cerebellum	Kidney	Striated muscle
Brain. Cerebral Cortex	Liver	Stomach
Brain Pituitary	Lung	Testis
Cervix	Lymph node	Thymus
Colon	Ovary	Thyroid
Duodenum	Pancreas	Ureter
Endothelium-artery	Placenta	Uterus
Esophagus	Prostate	

14G9: PLA2G1B 1C11: proPLA2G1B+PLA2G1B

14G9 and 1C11 14G9 only (=Tissue cross-reactivity)

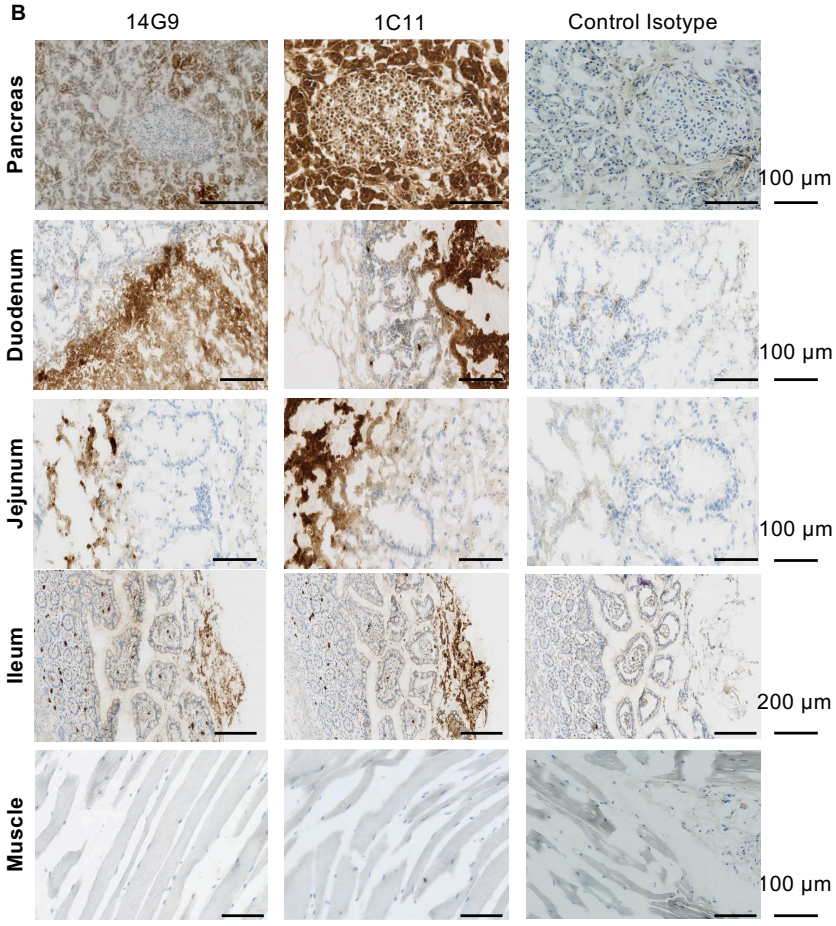

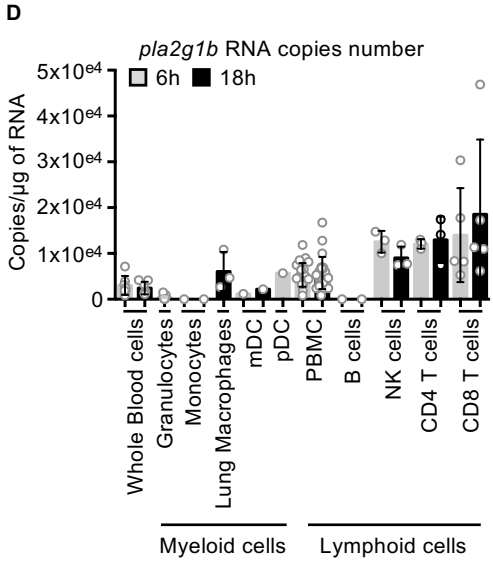

Supplemental Figure 8. Origin of hPLA2G1B – Low expression level in immune cells.
(**A**) Level of *pla2g1b* RNA in 19 human tissues and PBMCs. Gene expression is presented as the number of copies of *pla2g1b* per µg of total RNA and Ct value for PPIB. Data are shown as the mean ± SD of quadruplicate qRT-PCRs for *pla2g1b* and the mean of duplicate qRT-PCRs for *ppib*. The number of donors used to prepare the RNA samples were as follows: pancreas (n = 1), duodenum (n = 1), lung (n = 4), stomach (n = 2), adrenal gland (n = 6), liver (n = 3), kidney (n = 1), descending colon (n = 1), PBMCs (n = 24), brain (n = 5), trachea (n = 2), lymph Node (n = 1), thymus (n = 1), heart (n = 5), spleen (n = 2), placenta (n = 1), caval vein (n = 1), ascending colon (n = 1), spinal cord (n = 1), and skeletal muscle (n = 1). (**B**) Immunohistochemical analysis of total PLA2G1B (proPLA2G1B and active PLA2G1B, mAb 1C11) and active PLA2G1B (mAb 14G9) in human tissues. Staining by mAbs 14G9 and 1C11 on tissues expressing PLA2G1B among the 35 tissues tested is presented. IgG isotype, as well as skeletal muscle (*pla2g1b* RNA is not detected in muscle by qPCR), were used as negative controls. Data are representative of at least three independent experiments and different donors. (**C**) Summary of the analysis of proPLA2G1B and active PLA2G1B expression by tissue microarray (TMA), including 35 human tissues and four additional digestive tissues, duodenum, jejunum, ileum and rectum. Tissues were obtained from at least three independent donors with the exception of blood (one individual only). The 14G9 mAb shows a cross-reactivity with testis, since mAb 1C11 remains negative. (**D**) *Pla2g1b* RNA expression in immune cells after 6 and 18 h post-isolation. The number of donors used to prepare RNA samples were as follows: whole blood cells (n = 7 at 6 h and 18 h), granulocytes (n = 9 at 6 h), monocytes (n = 1 at 6 h and 18 h), lung macrophages (n = 3 at 18 h), mDCs (n = 1 at 6 h and 18 h), pDCs (n = 1 at 6 h), PBMCs (n = 22 at 6 h and 24 at 18 h), B cells (n = 1 at 6 h and 18 h), NK cells (n = 3 at 6 h and 18 h), CD4 T cells (n = 3 at 6 h and 18 h), and CD8 T cells (n = 5 at 6 h and 18 h). Data are shown as the mean ± SD of the number of copies of *pla2g1b* per µg of total RNA per donor.

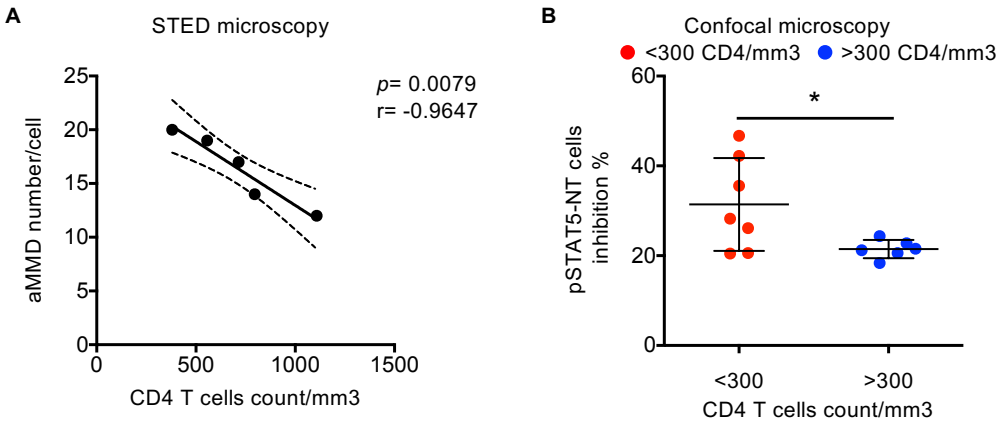

Supplemental Figure 9. Viremic patient (VP) plasma inhibitory activity is higher in viremic patients with low CD4 T-cell counts.

(**A**) The number of MMDs per cell induced by VP plasma negatively correlates with the CD4 T-cell count per mm^3 of VP. HD CD4 T cells were treated with 0.01% VP plasma from five different VPs and the number of MMDs per cell determined by CW-STED microscopy on an average of 50 cells per condition. Potential correlations were analyzed using the Pearson r test and linear regressions are presented with the 95% CI. (**B**) VP plasma from patients with low CD4 T-cell counts has higher inhibitory activity on pSTAT5 NT in HD CD4 T cells in response to IL-7. The inhibition of pSTAT5 NT was determined by confocal microscopy after treatment with 1% VP plasma. Results are presented as the percentage of inhibition obtained with plasma from VPs with <300 or >300 CD4 T cells count/mm^3. Experiments were performed on CD4 T cells from seven donors with two VP (VP#1-2) plasma samples from patients with <300 CD4 T cells/mm^3 (VP#1: n = 3 HD TCD4 cell donors and VP#2: n = 4 HD TCD4 cell donors) and three VP (VP#3-5) plasma samples from patients with >300 CD4 T cells/mm^3 (VP#3: n = 2 HD TCD4 cell donors, VP#4: n = 2 HD TCD4 cell donors, and VP#5: n = 2 HD TCD4 cell donors). Results are shown as the mean ± SD. The difference in the percentage of pSTAT5 NT obtained with the plasma of VPs with <300 CD4 T cells/mm^3 relative to that obtained with the plasma of VPs with >300 CD4 T cells/mm^3 was analyzed using the two-tailed unpaired *t*-test and $*p<0.05$.

Supplemental Table 1. Patients Characteristics

A. Characteristics of patients used for cell and plasma analysis

	HIV+	HIC	ART
Total patients	31	5	5
Age, Years (range)	36.4 (26.6-64.1)	54.7 (50.8-61.4)	36.7 (25.8-57.4)
Male, n (%)	20 (64.5%)	N.A	3 (60%)
Female, n (%)	11 (35.5%)	N.A	2 (40%)
CD4/mm^3 (range)	504 (8-1108)	852 (742-1050)	590 (401-902)
HIV-1 RNA /ml (range)	40,289 (3,870-352,767)	<50	<50

Median (Min-Max) are shown

B. Immunophenotyping of CD4 T cells from HD and VP

	HD	VP	p-values HD vs VP
Total donors	21	18	
% of T CD4+ in lymphocytes	39.5 (20.6-57.9)	19.9 (12.7-38.2)	< 0.0001
% CD45RA+ in T CD4+	28.9 (10.5-71.3)	34 (20.1-52.4)	0.0794
% CD45RA- in T CD4+	71.1 (27.6-89.5)	66 (47.6-79.9)	0.0677
% CD25+ in T CD4+	7.5 (3.76-12.5)	5.5 (3.25-10)	0.007
In T CD4+			
% CD127+	86.2 (69.4-92)	80.6 (54.5-87.4)	0.0072
MFI CD127	43.9 (22.8-66.9)	37 (9.2-57.5)	0.0434
In T CD4+ CD45RA+			
% CD127+	87 (73-96.3)	82.4 (48.5-96)	0.2661
MFI CD127	39.4 (22.9-54.4)	35.9 (9.2-54.1)	0.4866
In T CD4+ CD45RA-			
% CD127+	85.4 (74.4-90.4)	78.6 (56.3-84.4)	< 0.0001
MFI CD127	46.3 (22.3-71.1)	38.8 (9.13-62.3)	0.0203

Median (Min-Max) are shown

C. Characteristics of patients used for PLA2G1B dosage by ELISA

	HIV+	HIC	ART
Total patients	60	14	10
Age, Years (range)	41 (21-66)	45 (23-52)	52 (47-76)
Male, n (%)	30 (50%)	7 (50%)	7 (70%)
Female, n (%)	30 (50%)	7 (50%)	3 (30%)
CD4/mm^3 (range)	298 (15-1558)	637 (232-1006)	754.5 (566-1042)
HIV-1 RNA /ml (range)	18,812.45 (10,054-30,438)	<20	<20

Median (Min-Max) are shown

Supplemental Table 2. Crystal data PLA2G1B (Figure 4A).

Crystal parameters	
space group	p212121
cell dimensions, Å	*a*=30.61, *b*=58.95, *c*=122.10

Data statistics	
resolution, Å	42.2-1.90 (1.94-1.90)
unique reflections	18069 (1096)
multiplicity	4.1 (4.2)
Rmerge	0.119 (0.975)
Rpim	0.065 (0.529)
completeness, %	99.3 (98.0)
<I/sigma(I)>	8.8 (1.9)
$CC_{1/2}$	0.993 (0.580)

Rpim : precision-indicating R
$CC_{1/2}$: half-dataset correlation coefficient
(values in parentheses : highest resolution shell)

Refinement	
resolution, Å	42.41-1.90 (2.02-1.90)
R value, working set	0.175 (0.273)
Rfree	0.225 (0.354)
no. of reflections	18016 (2691)
protein residues	251
water molecules	339
chloride ions	4
r.m.s. deviations from ideal	
bond length, Å	0.010
bond angles, °	0.99
Ramachandran plot	
preferred regions, %	99.18
allowed regions, %	0.82

Supplemental Table 3. Anti-PLA2G1B antibodies.

Subclone	Antigen used for immunization	Isotype	Enzymatic activity (% of inhibition)	proPLA2G1B Kd (nM)	PLA2G1B Kd (nM)
#14G9	PLA2G1B	IgG1	95	1740 ± 7	0.338 ± 0.01
#1C11	PLA2G1B	IgG1	0	0.151 ± 0.012	0.064± 0.001
#6F7	PLA2G1B	IgG2a	0	N.D	N.D
#8G11	proPLA2G1B N-ter peptide	IgG2a	0	34.3 ± 2.7	> 10^4

N.D = Not determined

SUPPLEMENTAL MATERIAL

Study design and human sample collection.

The group of viremic patients (n = 31) included in the study of T lymphocytes and plasma consisted of patients with untreated chronic HIV-infection. These patients had never received antiretroviral drugs at the time of blood collection, their CD4 counts were > 300/mm^3, and their viral loads > 10,000 copies/mL (ANRS EP 33 and EP 20 studies). All blood samples from VPs were drawn at the Hôpital Bicêtre, Paris. Blood from HDs was obtained from healthy volunteers through the Etablissement Français du Sang (Centre Necker-Cabanel and St-Louis, Paris). Plasma samples from ART patients were drawn from individuals who had been receiving treatment for at least ten years. Their viral load was < 50 copies/mL for at least six months and their CD4 counts > 400/mm^3 at the time of blood collection. Plasma samples from HIV elite controller patients (HIC) were drawn at the Centre d'Infectiologie Necker-Pasteur, Paris, from individuals with a viral load of < 50 copies/mL 10 years after infection (ANRS EP36 study). Plasma samples were inactivated for HIV by heat-treatment as described in Goubran *et al.* (1) and stored at -80°C. To perform the correlation studies between CD4 counts or viral load with aMMD number /cell or the percentage of inhibition of pSTAT5-NT we added some samples from patients collected in the EP33 with CD4 counts < 300/mm^3 or viral loads < 10,000 copies/mL. Patient characteristics are described in Supplemental Table 1 parts (A) and (B).

ELISAs were performed on plasma from 119 healthy donors provided by Seralab, 14 HIC and 10 ART-treated and 60 HIV-infected patients collected at Hôpital de la Pitié-Salpêtrière see part (C) of the Supplemental Table 1.

Recombinant proteins and peptides.

Human proPLA2G1B, PLA2GIIA, PLA2GIID, and PLA2GX were produced in *E. coli* (purity > 99%). Active human PLA2G1B was produced in *E. coli* (purity > 98%), S2 cells (purity >

99%), or CHO-S cells (purity > 98%). Active porcine PLA2G1B and non-active mutant PLA2G1B H48Q were produced in *E. coli* (purity > 99%). Human H48Q PLA2G1B was produced in CHO-S cells (purity > 92%). HIV-1 MN gp41 recombinant protein was obtained from Antibodies Online (MN gp41 (565-771Delta642-725, ABIN2129703, purity > 95%). The 3S peptide NH2-PWNASWSNKSLDDIW-COOH and control peptide (CTL) NH2-PWNATWTQRTLDDIW-COOH were ordered from Covalab (purity > 98%). Cytokines used in the study consisted recombinant glycosylated human IL-7 (H4219, ACROBiosystems), human IL-2 (kind gift of Chiron, Emeryville, CA, USA), human IL-4 (H7291, Sigma-Aldrich), human IFN-α2 (11100-1, PBL Assay Science), and mouse IL-2 (AF-212-12, Preprotech).

Human T-cell isolation and culture.

CD4 and CD8 T cells were isolated from freshly collected blood samples from VPs or HDs. CD4 T cells were purified from PBMCs by negative selection using a CD4-purification kit (130-096-533, Miltenyi Biotec) (Figures 1 to 3). Unstimulated CD4 and CD8 T cells used for the experiments shown in Figures 4 to 6 and 8 were purified by negative selection from the same donor using the RosetteSep isolation kit (15062: CD4 T cells and 15063: CD8 T cells, Stemcell Technologies). Cells were cultured in microplates and activated for 15 min with 2 nM recombinant glycosylated human IL-7 where indicated. Cells were cultured at 37°C in a 5% CO_2 humidified atmosphere.

Detergent-resistant microdomains (DRMs) analysis by sucrose gradient and western blotting.

Purified primary CD4 T lymphocytes from HDs or VPs were stimulated, or not, with IL-7 (2 nM, 15 min). Harvested cells were cooled by the addition of ice-cold PBS, centrifuged, and lysed in 0.5% Triton X-100 buffer (50 mM Tris/HCl, pH 7.4, 5 mM EGTA, 5 mM EDTA, 30 mM NaF, 20 mM Na-pyrophosphate, 1 mM Na_3VO_4, 1 mM phenylmethylsulfonyl fluoride, 10

μM leupeptin). Lysate supernatant from 5×10^6 cells (300 μl) was loaded on the top of a 5-ml preformed 5–40% sucrose/Triton buffer gradient and centrifuged for 16 h at 50k rpm using a SW50 rotor in a Beckman ultracentrifuge. The tube contents were then collected into 18 fractions.

All samples were analysed by western blotting after SDS-PAGE separation on 7% acrylamide-bisacrylamide gels and transfer onto Hybond-ECL nitrocellulose membranes (GE Healthcare) overnight at 4°C. The membranes were blocked with BSA (Sigma) and incubated with primary antibodies. The primary antibodies were anti-IL-7R alpha (clone 40131, MAB306, R&D Systems) and anti-gamma c (clone TugH4, BD Biosciences). Anti-Flottilin-1 antibodies (clone 18, BD Biosciences) were used as a detergent-resistant membrane domain (DRM) marker. The membranes were washed in TBS/0.5% Tween 20 buffer before being incubated with horseradish peroxidase-coupled goat anti-mouse (Jackson) and goat anti-rat (Amersham Biosciences) secondary antibodies. The blots were revealed by ECL-plus western blotting detection reagents (GE Healthcare).

Analysis of the IL-7 receptor (IL-7R) diffusion rate at the surface of living CD4 T lymphocytes. CD4 T lymphocytes were purified from PBMCs, equilibrated 2 h in RPMI/10% FBS at 37°C, and transferred to poly-L-lysine coated coverslips in a glass bottom dish. The cells were pretreated at 37°C with either MMD inhibitors (cholesterol oxidase from *Streptomyces* sp., C8649, Sigma, COase: 25 min, 0.01-10 U/ml; sphingomyelinase from *Staphylococcus aureus*, S8633, Sigma, SMase: 5 min, 0.01-10 U/ml), or cytoskeleton inhibitors (CytD: 30 min, 0.01-100 μM; Col: 30 min 0.01-100 μM). A single cell was selected and IL-7 (2 nM) was added. The confocal volume was centered at the membrane level, at the top of the cell, opposite from the side in contact with the glass. Diffusion was observed during activation and autocorrelation (ACF) and cross-correlation (CCF) functions $G(\tau)$ were built from FCS and FCCS raw data,

respectively. ACF and CCF were fitted according to Schwille *et al.* (2).

Data on protein diffusion at the surface of living human CD4 T cells were acquired and analyzed, with or without MMD and cytoskeleton inhibitors, by spot variation FCS (3) using an inverted laser scanning confocal microscope (LSM510, Zeiss) combined with a ConfoCor2 FCS system (Zeiss), as previously described. Briefly, Rhodamine-6G (Rh6G, 252433, Sigma), anti-IL-7Rα-AF488 (clone 40131, FAB306G, R&D Systems), streptavidin-AlexaFluor488 (SAF488, S11233, Life Technologies), and IL-7Ralpha/anti-IL-7Ralpha-AF488 diffusion times were analyzed by autocorrelation of their fluorescence fluctuation intensities.

Effect of cytoskeleton inhibitors on phosphorylation and nuclear translocation of STAT (pSTAT5 NT) and analysis of cytoskeleton organization.

STAT phosphorylation and nuclear translocation after IL-7 stimulation (2 nM) were analyzed by microscopy in VP and HD CD4 T cells incubated with the cytoskeleton inhibitors colchicine (10 μM) plus cytochalasin D (20 μM) for 30 min. All pre-treatments and stimulations were performed at 37°C. Stimulation was stopped by addition of 4% PFA and incubation for 15 min at 37°C. Cells were then permeabilized for 20 min in a 90% methanol/water solution.

Cytoskeleton reorganization was analyzed by examining IL-7-induced actin and tubulin polymerization by STED microscopy. After immobilization on coverslips, the cells were activated with IL-7, or not. Activation was stopped by adding 1.5% PFA and incubation for 15 min at 37°C. For intracellular labelling, cells were permeabilized in ice-cold 90% methanol. The primary antibodies were rabbit anti-actin (sc-1616-R, Santa Cruz Biotechnologies) and mouse anti-tubulin (sc-31779, Santa Cruz Biotechnologies). Anti-mouse IgG-Chromeo494, anti-rabbit IgG-Chromeo494, and anti-rabbit IgG-Atto647 (Active motif) were used as secondary antibodies

Determination of apparent molecular weight and isoelectric point.

Apparent molecular weight was determined by size exclusion chromatography by loading 1.6 ml plasma onto a 85 ml Sephadex G100 column pre-equilibrated with PBS and then collecting 0.8 ml fractions of the eluate. The column was calibrated using a protein set (GE-Healthcare). Protein concentration was measured by the Bradford method. VP plasma previously filtered on a 100 kDa membrane and total VP plasma were tested and gave identical results.

The isoelectric point was determined by anion and cation exchange chromatography on 1-ml MonoQ and MonoS columns (GE-Healthcare), with elution by successive pH steps (ammonium carbonate/ammonium acetate buffers). The pH of each eluted fraction was measured and adjusted to pH 7.4 before being tested for their biological activity. Induction of the Bumpy T-cell phenotype (MMD and inhibition of pSTAT5 NT in response to IL-7) was measured in the corresponding fractions immediately after elution, as described in methods.

Bioinformatics – sequence selection of human protein candidates based on their molecular weight, isoelectric point, and amino-end secretion signal.

Protein datasets were selected from the neXtProt (Swiss Institute of Bioinformatics) database, curated from human proteins recorded in the Uniprot/SwissProt, and the Uniprot/variant splicing databases (Universal Protein Resource). Molecular weights and isoelectric points were calculated from the protein sequences using online tools from the Bioinformatics Resource portal at Expasy (Swiss Institute of Bioinformatics). Amino-end signal peptides were detected using the online SignalP 4.1 Server (Center for Biological Sequence Analysis, Technical University of Denmark, DK).

Selection / Databases[a]	Uniprot[b]	Uniprot_splic[c]	neXtProt[d]
human	20233	16758	36830
human / MW 10 - 20K	2406	1849	4120
human / MW 10 - 20K / Ip 6.00 - 8.00	341	288	604
human / MW 10 - 20K / Ip 6.00 - 8.00 / signalP	60	43	103

[a]selection criteria: human origin, molecular weight cutoff, isoelectric point cutoff, signal peptide predicted with signal (v4.0)
[b]Uniprot/swiss-prot: protein sequence database (unprocessed precursor sequences)
[c]Uniprot/splice variant: protein sequence database (unprocessed precursor sequences)
[d]neXtProt protein: sequence database (unprocessed precursor sequences)

Proteomics – characterization of protein candidates from active plasma fractions.

Plasma were separated from whole blood samples after two successive centrifugations, first at 1,800 rpm for 10 min to separate cells and then at 3,500 rpm 30 min to remove cell debris and platelets. Plasma was then filtered through a 0.22 µm-filter (Millipore). Proteins were separated from 1.6 ml plasma samples by size-exclusion through a Sephadex 100 column (80 cm long, 0.5 ml/min) equilibrated in 50 mM ammonium carbonate buffer, pH 8. All fractions were lyophilized and stored at -80°C. Fractions were analyzed by CLIPP proteomics using MS analysis (Clinical and Innovation Proteomic Platform, University of Bourgogne, Dijon, France). The MS data were generated in biological triplicates from plasma samples of six blood donor: three healthy volunteers and three HIV-infected patients.

Selected fractions from plasma separation using size exclusion chromatography were pooled, lyophilized, resuspended in milliQ water, sonicated, and vortexed. Proteins were reduced using 10 mM *TCEP* (tris (2-carboxyethyl)phosphine) in 0.1 M NH_4HCO_3 buffer (30 min, 37°C) and then alkylated with 55 mM iodoacetamide (20 min, RT). Proteins were digested by trypsin (Promega, gold mass spectrometry grade, 20 ng/µL final concentration, 3 h, 37°C). Proteolysis was stopped by adding formic acid (0.1% final). Digestion of rat serum albumin (2 pmoles) was performed in parallel as a control. Digestions were validated by analyzing 0.5 µL trypsin-treated samples using MALDI-TOF/TOF (UltrafleXtreme, Bruker Daltonics).

Digested samples were analyzed by nano-liquid chromatography separation (LC), electrospray ionization of peptides (ESI), and separation through an orbital ionic trap (OrbiTrap ELITE, ThermoScientific). LC was performed by injecting 2 µg peptide mix through a C18 column (Dionex, 15 cm long, 75 µm diameter, 2 µm beads) on a nano-HPLC (Ultimate 3000, Dionex) and running a 2-80% acetonitrile gradient in 0.1% formic acid. MS analysis was performed by ESI-OrbiTrap from 400 to 1700 m/z. The peptides providing the 20 most intense m/z peaks were automatically selected and fragmented for analysis on an OrbiTrap (MS/MS). MS data were managed and analyzed using Proteome Discoverer Software 1.4 (Thermo Scientific). Proteins were identified using the Mascot program (Matrix Science) for human sequences in the SwissProt database (Universal Protein Resource) with the following parameters: one uncut trypsin cleavage site allowed, carbamidomethylation of cysteine and possible oxidation of methionine, and a mass tolerance of 10 ppm for MS and 0.6 Da for MS/MS.

Peptide separation and MS and MS/MS analysis were controlled and validated by injecting 100 fmoles of digested BSA.

Peptides from plasma fractions were independently injected and analyzed three times using a nanoLC-ESI-OrbiTrap providing 3,000-6,000 MS spectra series. The 20 peptides providing the highest intensity of their m/z peaks were fragmented and their fragments analyzed by a second MS run. A total of 18,000-35,000 MS/MS spectra were acquired for each run.

The raw MS and MS/MS data series were independently analyzed for each run, scoring the representation of peptides issued from the data set of 103 selected proteins from the bioinformatics analysis with the standard parameters used for Mascot analysis: one uncut trypsin cleavage site allowed, carbamidomethylation of cysteine and possible oxidation of methionine, mass tolerance of 10 ppm for MS and 0.6 Da for MS/MS. Three scores were calculated for each of the 103 proteins and are reported in Supplemental Figure 2D: number of

peptides matching with m/z peaks in MS spectra series unique amongst all peptides from the 103-protein dataset, neXtProt dataset (human-dataset).

Active human PLA2G1B crystallization, structure determination, and refinement.

Screening of the crystallization conditions was carried out by the vapor diffusion method with a MosquitoTM nanolitre-dispensing system (TTP Labtech, UK). Sitting drops were set up using 400 nl of a 1:1 mixture of PLA2G1B at 5.3 mg/ml and crystallization solutions (672 different commercially available conditions) equilibrated against a 150-µl reservoir in multiwell plates (Greiner Bio-One). The crystallization plates were stored in a RockImager1000^{TM} (Formulatrix, USA) automated imaging system to monitor crystal growth. Crystals were obtained at 18°C in solutions containing 32% (w/v) PEG4K, 0.8 M Lithium chloride, and 100 mM Tris-HCl pH 8.5. Single crystals were flash-cooled in liquid nitrogen using a 1:1 mixture of Paratone-N and paraffin oil as cryoprotectant. X-ray diffraction data were collected on the PROXIMA-1 beamline at the SOLEIL synchrotron (Saint-Aubin, France). The diffraction images were integrated with XDS (4), and crystallographic calculations were carried out with programs from the CCP4 program suite (5). The structure was solved by molecular replacement with Phaser (6) using porcine pancreatic PLA2 (pdb code 2B00) as a template. The structure was refined with Buster (7) and manual adjustments were made to the models with Coot (8). The crystallographic parameters, data statistics, and refinement statistics are shown in Supplemental Table 2. Atomic coordinates and structure factors have been deposited in the RCSB Protein Data Bank with pdb code 6Q42.

Lipidomic analysis of primary human CD4 and CD8 T cells.

CD4 T cells (2 x 10^6) and CD8 T cells (2 x 10^6) from three healthy donors were purified by negative selection as described above using the RosetteSep isolation kit (Stemcell

Technologies). The percentage of CD4 T cells and CD8 T cells was determined by flow cytometry.

	HD#1	HD#2	HD#3
% T CD4 in T CD4	97.6	97.5	93.2
% T CD8 in T CD4	0.004	0.006	0.003
% T CD8 in T CD8	90	89.3	92.5
% T CD4 in T CD8	0.024	0.87	0.044

Total lipid extracts from purified CD4 and CD8 cells were obtained using the Folch method (9), with modifications. The lipidomic analysis by mass spectrometry, including data treatment, has been published (10). The percentage of lipids was calculated based on chromatographic peak areas (a.u) for each lipid relative to the sum of the chromatographic peak areas for all lipids for each donor. Statistical differences of lipid content between CD4 and CD8 T cells were analyzed in CD4 T cells isolated from one donor relative to CD8 T cells isolated from the same donor and results obtained from three independent donors were analyzed with a two-tailed paired t-test. Lipid species among a total of 330 detected lipid species with $p<0.05$ are presented in Supplemental Figure 4E.

ELISA Quantification of active PLA2G1B and proPLA2G1B levels in plasma from patients and healthy donors.

Antibodies specific for active PLA2G1B were generated at BIOTEM (France) by immunization of OF1 mice with recombinant active human PLA2G1B that was produced in *E. coli*. Antibodies specific for proPLA2G1B were also generated at BIOTEM by immunization of OF1 mice with an N-terminal PLA2G1B peptide conjugated to KLH containing the PLA2G1B propeptide sequence (DSGISPRAVWQFRKMIKC). From among 36 mAbs, we selected those

that inhibited the enzymatic activity of PLA2G1B (14G9) or bound specifically to proPLA2G1B (8G11) or both active PLA2G1B and proPLA2G1B (1C11, 6F7). The affinity constants (Kd) of the binding of these antibodies to proPLA2G1B and PLA2G1B were determined by surface kinetics on a real-time biosensor using surface plasmon resonance (BIAcore™, Molecular Biophysic platform, Institut Pasteur, France) and are presented in Supplemental Table 3.

We developed ELISAs to specifically detect active PLA2G1B and proPLA2G1B at Theradiag (France).

PLA2G1B protein expression in human tissues.

Immunohistological analyses were performed at Histalim (France) on frozen normal human tissues provided by Histalim with antibodies that bind specifically to active PLA2G1B (14G9), or both active PLA2G1B and proPLA2G1B (1C11, see Methods for details) and a control mouse IgG1 isotype. The procedure to specifically detect active PLA2G1B by immunohistochemistry with 14G9 was set-up using CHO cells that express only active human PLA2G1B relative to CHO cells that express human proPLA2G1B or those that were not transfected. Specific labelling of active PLA2G1B with 14G9 was observed with 0.3 and 1 µg/ml of antibody. The donor tissues were qualified by performing hematoxylin-eosin (H&E) staining and vimentin immunohistochemistry. Staining was performed on 5 to 10-µm sections stored at -80°C. The sections were thawed for 15 to 60 min, post-fixed in formol for 20 min, and labelled with 14G9 (1 µg/ml for all tissues except muscle, which was labelled with 5 µg/ml), 1C11 (0.1 µg/ml for all tissues), and control isotype (5 µg/ml for pancreas and muscle, and 1 µg/ml for other tissues). In total, 35 tissues were analyzed using tissue microarrays (TMAs) containing 30 tissues from three unrelated donors, one blood specimen, and additional sections of duodenum, jejunum, ileum and rectum from three unrelated donors.

Immunodepletion with anti-PLA2G1B antibodies and anti-gp41 antibodies to study plasma cofactor activity.

Plasma cofactor activity was evaluated by immunodepleting endogenous PLA2G1B and gp41 with specific antibodies. Briefly, 1 ml VP or HD plasma was incubated with 5 µg of the mouse anti-PLA2G1B mAb 6F7 or control isotype (Mouse IgG1, 16-4714-85, Thermofisher), to immunodeplete PLA2G1B, or with 100 µg goat anti-gp41 polyclonal antibody (PA1-7219, Thermofisher) or the control goat polyclonal antibody (preimmune, AB108-C, R&D Systems), to immunodeplete gp41, in 1.5-ml Eppendorf tubes overnight (Test tube-rotor, 34528, Snijders, Netherland) at 4°C. As the goat anti-gp41 pAb initially contained 0.1% sodium azide, it was washed five times with PBS on 10 kDa Amicon (051828, Millipore) spin filters by centrifugation at 16,100 x *g* for 2 min at 4°C to remove the sodium azide before proceeding to immunodepletion. The normal goat IgG control was treated similarly as the anti-gp41 pAb. Then, 200 µl Protein G Sepharose 4 Fast Flow beads (17-0618-01, GE healthcare), that had been washed three times in PBS/1%BSA, was added to each sample and the samples incubated for 3 h at 4°C. Beads were removed by centrifugation of the samples at 400 x *g* for 2 min at 4°C, collection of the supernatant then centrifugation at 16,100 x *g* for 15 min at 4°C.

Antibodies specific for the 3S sequence (PWNASWSNKSLDDIW) in HIV-1 MN strain gp41 were generated at BIOTEM (France) by immunization of OF1 mice with the peptide NH2-C-PWNASWSNKSLDDIW-COOH conjugated to KLH. We selected the anti-3S gp41 mAb 1C5 (IgG2b/k) based on its high affinity for the 3S peptide and MN gp41 recombinant protein by ELISA. The 1C5 mAb and goat anti-gp41 pAb bind specifically to recombinant gp41 but not gp120 (Supplemental Figure 7).

VP or HD plasma (500 µl) from three VPs and three HDs were fractionated on Amicon spin filters with a 30 kDa cut-off (051850, Millipore) and then a 10k Da cut-off (051828, Millipore). The 10-30 kDa fraction was collected and treated with control isotype (Mouse IgG2b/k, 16-

4732-85, Thermofisher) or gp41 was immunodepleted with 100 µg of 1C5 mAb as described above.

Characterization of monoclonal 1C5 and goat pAb anti-gp41 specificity on gp41 and gp120 recombinant proteins.

Recombinant gp41 and gp120 were produced in S2 cells. Microtiter plates were coated in triplicate with 10 µg/well of either recombinant gp120 or recombinant gp41 in carbonate buffer pH 9.6. After overnight incubation at 4°C, nonspecific binding sites were blocked with Pierce blocking buffer (37572, Pierce). Anti-3S mAb 1C5 was added to a final dilution of 1 µg/well in blocking buffer. Bound antibody was detected by interaction with a goat-anti mouse HRP-conjugated antibody, followed by the addition of 100 µL/well TMB substrate (UP664781, Interchim). The reaction was stopped by adding 50 µL 0.1 M H_2SO_4 and the O.D. $_{450nm}$ was measured using a Tecan Infinite M1000 Pro.

For western blot analysis, 500 ng or 1 µg of recombinant protein was run on 4%–20% Tris-Bis SDS-PAGE (BIO-RAD) gels under reducing conditions. Antigens were transferred to PVDF membranes (BIO-RAD) using a Trans-Blot Turbo (BIO-RAD). After blocking nonspecific binding sites with 5% milk/0.05% tween 20 in PBS, antibody binding was tested at 1µg/ml for 1C5 and up to 5 µg/ml for the polyclonal anti-gp41(PA1-7219, Thermofisher). Goat anti-mouse (31430, Pierce) and donkey anti-goat (705-035-003, Jackson Immunoresearch) HRP-conjugated antibodies were used at a 1:10,000 dilution. Detection occurred directly on the membrane using SuperSignal West Pico Plus Substrate (34580, ThermoScientific).

Quantification of pla2g1b RNA by quantitative real-time PCR (qRT-PCR) in healthy donor and HIV$^+$ Viremic Patient PBMCs, tissues, and immune cells.

RNA of PBMCs from viremic HIV patients were collected by José Alcami (National Center of Microbiology. Instituto de Salud Carlos III, Spain). Healthy donor PBMC RNA was isolated

from PBMCs isolated from whole blood bags containing citrate, freshly collected at the "Etablissement Français du Sang" (EFS), using lymphocyte separation medium (CMSMSL01-01, Eurobio).

Human tissue RNAs consisted of MVP total RNAs from Agilent Technologies (540023: pancreas, 540131: duodenum, 540019: adult Lung, 540133: adrenal gland, 540037: stomach, 540013: kidney, 540017: human liver, 540145; trachea, 540035: spleen, 540125: descending colon, 540123: ascending colon, 540021: lymph node, 510121: vena cava, 540025: placenta, 510141: thymus, and 540029: skeletal muscle) and Total RNA from Biochain (R1234004-P: Normal Tissue 5 Donor Pool Adrenal Gland, R1234035-P: Normal Tissue 5 Donor Pool from Brain, R1234122-P: Normal Tissue 5 Donor Pool from Heart, R1234234-50: Human Normal Tissue from Spinal Cord). qPCR data for the adrenal gland is shown as the mean of quadruplicate qRT-PCR ± SD from both adrenal gland RNA samples.

Whole blood cell RNA was isolated from healthy donor blood after collection in heparin tubes (Etablissement Français du Sang, EFS). RNA was extracted using the QIAamp RNA Blood Mini Kit (52304, Qiagen). Lung macrophage RNA was a kind gift from C. Abrial and L. Touqui (Institut Pasteur, France). RNA of VP and HD PBMCs was prepared as described below.

Immune cells were isolated from healthy donor whole blood bags containing citrate, freshly collected at the EFS, using lymphocyte separation medium (CMSMSL01-01, Eurobio, PBMCs, granulocytes), the Pan Monocyte isolation kit (Monocytes (CD14+): 130-096-537, Miltenyi Biotec), and the Easy Sep kit from Stemcell (pDCs ($CD45RA^+$ $CD304^+$): 19062, Human Plasmacytoid DC enrichment kit; mDCs (Lin^- $CD11c^+$ $HLA\text{-}DR^{+)}$: 19061, Human Myeloid DC enrichment kit; NK cells ($CD56^+$ $CD3^-$ $CD14^-$):19055, Human NK cell enrichment kit; B cells ($CD19^+$ $CD304^-$): 19054, Human B cell enrichment kit; CD4 T cells ($CD3^+$ $CD4^+$): 17952, Human CD4 T cell isolation kit; and CD8 T cells ($CD3^+$ $CD8^+$): 17953, Human CD8 T cell

isolation kit). Red blood cells were removed from granulocytes by treating the cells with BD Pharm lyse Buffer (555899, BD Biosciences).

Cell purity was checked by flow cytometry with specific antibodies as follows: pDC (CD45RA-FITC, 555488, BD biosciences; CD304-APC, 130-098-874, Miltenyi Biotec), mDC (Lin-FITC, 348701, Biolegend; CD11c-APC, 301614, Biolegend; HLA-DR-PE, clone TU36, 555812, BD Biosciences), B cells (CD19-RPE, clone HD37, R0808, Dako; CD304-APC, 130-098-874, Miltenyi Biotec), NK cells (CD14-RPE, MHCD1404, Molecular Probes; CD56-APC, clone MME-188, 304610, Biolegend; CD3-V500, clone UCHT1, 561416, BD Biosciences), CD4 T cells (CD4-PerCP, clone SK3, 345770, BD Biosciences; CD69-FITC, 347823, BD biosciences; CD3-V500, clone UCHT1, 561416, BD Biosciences), CD8 T cells (CD8-APC, clone DK25, C7227, Dako; and CD3-V500, clone UCHT1, 561416, BD Biosciences).

cDNA was obtained from 1 µg total RNA as follows: total RNA was extracted using QIAshredder (79654, Qiagen) and the RNeasy Kit (74104, Qiagen). Extracted RNA was treated with DNase I (RNase-Free DNase Set, 79254, Qiagen) and reverse transcribed using SuperScript III reverse transcriptase (18080-044, Invitrogen) according to the manufacturer's instructions. Specific TaqMan probes from Applied Biosystems were used to quantify *pla2g1b* (Hs00386701_m1) *b2m* (Hs00984230_m1), *ppib* (Hs00168719_m1), and *β-actin* (Hs01060665_g1) mRNA levels by qRT-PCR using TaqMan Universal Master Mix II with UNG (4440038, Thermofisher), according to the manufacturer's instructions. Quadruplicate Ct values for *pla2g1b* were analyzed using the comparative Ct (ΔΔCt) method (Applied Biosystems). The relative amount of mRNA ($2^{-\Delta\Delta Ct}$) was obtained by normalizing against the *b2m*, *ppib*, and *β-actin* endogenous references in the comparison of VP and HD PBMCs (Figure 8C). The relative amount of mRNA ($2^{-\Delta\Delta Ct}$) was obtained by normalizing against the endogenous *ppib* reference level in the tissues studied (Supplemental Figure 8A) and the endogenous *b2m* reference level for immune cells (Supplemental Figure 8D). The levels of

pla2g1b are presented as copies of *pla2g1b* per µg of RNA, based on a standard curve obtained with a pCDNA3.1 expression vector encoding human proPLA2G1B.

Preparation and study of human naïve and memory CD4 T-cell subpopulations.

For the analysis of the differential effect of VP plasma and PLA2G1B on human naïve and memory CD4 T cells, the subpopulations were prepared from the same healthy donor by negative selection (StemCell isolation kits) and the effect compared to that of total CD4 T cells from the same donor. The effect on pSTAT5 NT was analyzed by confocal microscopy after CD45RA (clone HI100, 304102, Biolegends), CD45RO (clone UCHL1, 304202, Biolegends), or CD25 (AF-223-NA, R&D Systems) and pSTAT5 labelling and compared to the effect on total CD4 T cells from the same healthy donor.

Study of the effect of PLA2G1B on IL-7R (CD127) expression on human CD4 CD45RA+ and CD4 CD45RA- T-cells.

Isolated CD4+ T cells were equilibrated overnight in the medium described above and treated with or without 1 μM of hPLA2G1B or H48Q for 30 min at 37°C. Cells were then stained for live and dead cells with Zombie Nir Fixable Viability Kit (423106, Biolegend). Fc receptors were blocked with the human TrueStain FcX blocking solution (422302, Biolegend) for 15 min at 4ºC and cells were stained for 30 min at 4ºC with antibodies against: CD4-FITC (clone AI61A1, ref 357406, Biolegend), CD45RA-V450 (clone Hl100, ref 560382, BD Biosciences), CD45RO-BV650 (clone UCHL1, ref 563750, BD Biosciences), CD127-APC (clone A019D5, ref 351316, Biolegend) and its associated isotype control. Cells were analyzed with a MACSQuant cytometer (Miltenyi Biotec) and with the FlowJo software, version 10 (Tree Star). CD127 expression on Figure 5G is presented as anti-CD127 MFI minus isotype control MFI.

Mice.

Eight- to ten-week-old SOPF C57BL/6J male mice were purchased from Charles River Laboratory (France). Animals were housed in specific pathogen-free conditions and maintained under barrier conditions in individually ventilated cages in accredited animal facilities at the Institut Pasteur.

Preparation and study of the mouse CD8 T cell population.

Mouse CD8 T cells were isolated from splenocytes prepared as described in Methods using the EasySep isolation kit (19853, Stemcell Technologies). The nuclear translocation of phospho-STAT5 was analyzed by confocal microscopy as previously described. Mouse CD8 T cells were stained with rat anti-mouse CD8 (clone 53-6.7, 14-0042-85, eBioscience) labelled with chicken anti-rat-AlexaFluor 488 (A21470, Life Technologies).

Study of the effect of PLA2G1B on phosphatidylserine at the surface of mouse CD4 T cells.

For the Annexin V experiments, murine CD4 T cells were stained with AlexaFluor488-conjugated antibodies against CD4 (557667, clone RM4-5; BD Biosciences) for 30min at 4°C and the Zombie Violet Fixable Viability Kit (0.25µL/ test) (423114, Biolegend) and Annexin V-APC (2,5µL/test) (640941, Biolegend) for 15 min at RT. Cells were analyzed with a MACSQuant cytometer (Miltenyi Biotec) and FlowJo software, version 10 (Tree Star).

Determination of the effect of PLA2G1B on Mouse CD4 T cell CD25 expression, survival, and proliferation in response to anti-CD3/CD28 stimulation.

CD4 T cells were isolated from the spleens of male C57BL/6J mice (8-10 weeks old) by negative selection using the Easy Sep™ Mouse CD4 T cell isolation kit (19852, StemCell Technologies). Isolated CD4 T cells were labelled with a cell proliferation marker (135-1202,

Cytotrack Cell Proliferation Assay Kit, BioRad) using the manufacturer's protocol. Cells were cultured in RPMI with 5% FBS/1% L-glutamine/1% Penicillin/Streptomycin/0.1% HEPES, with or without various concentrations of hPLA2G1B (from 125 nM to 1 µM; 125 nM for the inhibition experiment with anti-hPLA2G1B) for 30 min at 37°C. Cells were then activated with anti-CD3/CD28 (11456D, Dynabeads, mouse T-cell activator (Gibco) at a ratio of 1 bead:1 cell) with 50 IU/ml recombinant murine IL-2 and/or treated with anti-hPLA2G1B or IgG1 isotype control at 1.25 µM. Media, cytokine, hPLA2G1B and/or anti-hPLA2G1B or IgG1 isotype control (1C11, an anti-PLA2G1B mAb that does not inhibit PLA2G1B activity, see Supplemental Table 3) were replenished after two days of culture and the cells were analyzed by FACS after five days of activation.

Murine CD4 T cells were stained for live and dead cells using the Zombie Nir Fixable Viability Kit (423106, Biolegend). Fc receptors were blocked with an anti-CD16/CD32 antibody (553141, clone 2.4G2; BD Biosciences) for 15 min at 4ºC and cells were stained for 30 min at 4ºC with antibodies against: CD4-AlexaFluor488 (557667, clone RM4-5; BD Biosciences), CD25-PE (553866, clone PC61; BD Biosciences), and isotype controls. Cells were analyzed with a MACSQuant cytometer (Miltenyi Biotec) using FlowJo software, version 10 (Tree Star).

In vivo neutralization of PLA2G1B activity by anti-PLA2G1B mAb 14G9 or PLA2G1B/BSA immunization.

Briefly, 20 male C57BL/6J SOPF mice were divided into four experimental groups. Two groups were injected i.p. at T0 with 1 mg isotype control mAb (human IgG1, BP0297, BioXCell, group 1) or neutralizing anti-PLA2G1B mAb 14G9 (group 2) and received 100 µg PLA2G1B at T + 2 h. Two groups received vehicle only (PBS) or 100 µg PLA2G1B at T + 2 h. At T + 5 h (3 h post-PLA2G1B injection), mouse splenocytes were prepared using a gentleMACS Dissociator (program m_spleen_01), the CD4 T cells isolated by negative selection using the EasySep isolation kit (19852, Stemcell Technologies), and phospho-STAT5

analyzed by confocal microscopy, as described above. pSTAT5 was then revealed by staining with rabbit anti-pSTAT5 labelled with donkey anti-rabbit-AlexaFluor 555 (A31572, Life Technologies) and the mouse CD4 T lymphocytes cells were stained with rat anti-mouse CD4 (14-0042-85, clone RM4-5, eBioscience) labelled with chicken anti-rat-AlexaFluor 488 (A21470, Life Technologies).

The inhibitory effect of PLA2G1B on CD4 T cells was further investigated in vivo by immunizing mice against PLA2G1B/BSA (anti-hPLA2G1B Immunized) or BSA alone (ctrl). Twenty male C57BL/6J SOPF mice were randomized between one control group (Ctrl mice, 10 animals) and one immunized group (anti-hPLA2G1B Immunized mice, 10 animals). The Ctrl and anti-hPLA2G1B Immunized mice were injected three times (prime + two boosts) i.p., at three-week intervals between each injection, using a final volume of 200 µL: for Ctrl mice, 100 µL BSA (50 µg BSA for prime, 20 µg BSA for boost + 100 µL adjuvant); for anti-hPLA2G1B Immunized mice, 100 µL PLA2G1B linked to BSA (50 µg PLA2G1B for prime, 20 µg PLA2G1B for boost + 100 µL adjuvant). Complete Freund's Adjuvant (CFA; Sigma-Aldrich) was used for the prime injection. Incomplete Freund's Adjuvant (IFA; Sigma-Aldrich) was used for the two booster injections. Seven days after the second booster injection, blood samples (~100 µL) were harvested by retro-orbital vein puncture into EDTA-coated microtubes (Microvette® CB300 K2E) for screening of PLA2G1B neutralizing antibodies. The mean titer of the anti-hPLA2G1B-immunized group was 1:10,000. Titers were determined as the highest dilution that exceeded a threshold of three standard deviations above the background. Seven days after collecting plasma samples the animals were inoculated with 100 µg PLA2G1B i.p. to assess neutralization in vivo. Half of the ctrl and anti-hPLA2G1B-immunized mice were euthanized 3 h later, whereas the other half was processed 24 h after PLA2G1B injection. The spleens were harvested immediately after euthanasia. CD4 T cells were isolated and pSTAT5 NT analyzed as described in the previous paragraph.

SUPPLEMENTARY MATERIAL REFERENCES

1. Goubran HA, Burnouf T, Radosevich M. Virucidal heat-treatment of single plasma units: a potential approach for developing countries. *Haemophilia.* 2000;6(6):597–604.

2. Bacia K, Kim SA, Schwille P. Fluorescence cross-correlation spectroscopy in living cells. *Nat Methods.* 2006;3(2):83–89.

3. He H-T, Marguet D. Detecting Nanodomains in Living Cell Membrane by Fluorescence Correlation Spectroscopy. *Annu Rev Phys Chem.* 2011;62(1):417–436.

4. Kabsch W. Integration, scaling, space-group assignment and post-refinement. *Acta Crystallogr Sect D Biol Crystallogr.* 2010;66(2):133–144.

5. Winn MD, et al. Overview of the *CCP* 4 suite and current developments. *Acta Crystallogr Sect D Biol Crystallogr.* 2011;67(4):235–242.

6. McCoy AJ. Solving structures of protein complexes by molecular replacement with *Phaser* *Acta Crystallogr Sect D Biol Crystallogr.* 2007;63(1):32–41.

7. Smart OS, et al. Exploiting structure similarity in refinement: automated NCS and target-structure restraints in *BUSTER*. *Acta Crystallogr Sect D Biol Crystallogr.* 2012;68(4):368–380.

8. Emsley P, Lohkamp B, Scott WG, Cowtan K. Features and development of *Coot*. *Acta Crystallogr Sect D Biol Crystallogr.* 2010;66(4):486–501.

9. Folch J, Lees M, Slonae Stanley GH. A simple method for the isolation and purification of total lipides from animal tissues. *J Biol Chem.* 1957;226(1):497–509.

10. Seyer A, Boudah S, Broudin S, Junot C, Colsch B. Annotation of the human cerebrospinal fluid lipidome using high resolution mass spectrometry and a dedicated data processing workflow. *Metabolomics.* 2016;12:91.